Syncoilin modulates peripherin filament networks and is necessary for large-calibre motor neurons

W. Thomas Clarke[1,*], Ben Edwards[1,*], Karl J. A. McCullagh[1,‡], Matthew W. Kemp[1,§], Catherine Moorwood[1,¶], Diane L. Sherman[2], Matthew Burgess[1,] and Kay E. Davies[1,‡‡]**

[1]MRC Functional Genomics Unit, Department of Physiology, Anatomy and Genetics, University of Oxford, South Parks Road, Oxford, OX1 3PT, UK
[2]Centre for Neuroscience Research, The University of Edinburgh, Summerhall, Edinburgh, EH9 1QH, UK

*These authors contributed equally to this work
‡Present address: Regenerative Medicine Institute, National Centre for Biomedical Engineering Science, National University of Ireland, Galway, Ireland
§Present address: School of Women's and Infants' Health, Faculty of Medicine, Dentistry and Health Sciences, The University of Western Australia, Western Australia, WA 6009
¶Present address: Department of Physiology and Pennsylvania Muscle Institute, University of Pennsylvania School of Medicine, Philadelphia, PA 19104, USA
**Present address: Botnar Research Centre, Institute of Musculoskeletal Sciences, Nuffield Department of Orthopaedics, Rheumatology and Musculoskeletal Sciences, University of Oxford, Oxford OX3 7LD, UK
‡‡Author for correspondence (kay.davies@dpag.ox.ac.uk)

Accepted 20 April 2010
Journal of Cell Science 123, 2543-2552

doi:10.1242/jcs.059113

Summary

Syncoilin is an atypical type III intermediate filament (IF) protein, which is expressed in muscle and is associated with the dystrophin-associated protein complex. Here, we show that syncoilin is expressed in both the central and peripheral nervous systems. Isoform Sync1 is dominant in the brain, but isoform Sync2 is dominant in the spinal cord and sciatic nerve. Peripherin is a type III IF protein that has been shown to colocalise and interact with syncoilin. Our analyses suggest that syncoilin might function to modulate formation of peripherin filament networks through binding to peripherin isoforms. Peripherin is associated with the disease amyotrophic lateral sclerosis (ALS), thus establishing a link between syncoilin and ALS. A neuronal analysis of the syncoilin-null mouse (*Sync*$^{-/-}$) revealed a reduced ability in accelerating treadmill and rotarod tests. This phenotype might be attributable to the impaired function of extensor digitorum longus muscle and type IIb fibres caused by a shift from large- to small-calibre motor axons in the ventral root.

Key words: Syncoilin, Peripherin, Intermediate filaments, Amyotrophic lateral sclerosis, Neurons, Ventral root, Axon calibre

Introduction

Syncoilin is an atypical type III intermediate filament (IF) protein that lacks the key features of IFs, including the L1 linker domain and a periodic distribution of charged residues across the rod domain (Kemp et al., 2008). Syncoilin has never been observed under normal conditions to form filament structures either alone or with other IF proteins, but thick syncoilin filament-like structures are known to form in some myopathies where syncoilin upregulation occurs (Brown et al., 2005).

Syncoilin is highly expressed in skeletal and cardiac muscle where it interacts with α-dystrobrevin, a component of the dystrophin-associated protein complex, and desmin, the major IF protein expressed in mature myocytes (Newey et al., 2001; Poon et al., 2002). Knockout animal models for both α-dystrobrevin and desmin have a mild muscular dystrophy (Grady et al., 1999; Li et al., 1996). Myofibre regeneration in α-dystrobrevin (*Dtna*)-null mice results in the upregulation of syncoilin, but syncoilin expression is reduced and completely lost from the neuromuscular-myotendinous junctions in desmin (*Des*)-null mice (McCullagh et al., 2007). Given the alterations to syncoilin expression in these models of muscle myopathies, mice null for syncoilin (*Sync*$^{-/-}$) show surprisingly few signs of disease. *Sync*$^{-/-}$ mice have an unremarkable muscle phenotype with the exception of a reduction in maximal-force capacity in EDL muscle (McCullagh et al., 2008; Zhang et al., 2008) and an increase in serum levels of creatine kinase after a period of enforced endurance running (McCullagh et al., 2008).

Two new isoforms for syncoilin (Sync2 and Sync3) have been identified in addition to the original and dominant isoform in muscle (Sync1). These isoforms are spliced from a single gene and differ only in their C-terminal ends. Syncoilin isoforms are differentially upregulated during atrophy and regeneration, suggesting distinct but possibly significant functions for syncoilin (Kemp et al., 2008).

In addition to their expression in muscle, IFs of the type III, IV and V families are also expressed in neuronal tissues (Jing et al., 2007; Lariviere and Julien, 2004). Most notably, similarly to syncoilin, peripherin is a type III IF protein with several known isoforms. Per58 is generated by all nine exons of the human and mouse gene and forms filaments; the Per45 isoform does not form filaments and is generated using a downstream in-frame initiation codon. The absence of Per45 or disruption of Per45 to Per58 ratios has been shown to disrupt the normal peripherin filamentous structures (McLean et al., 2008). Two peripherin isoforms are associated with amyotrophic lateral sclerosis (ALS): aggregate-inducing Per28 is upregulated in patients with ALS and is associated with round inclusions in disease pathology (Xiao et al., 2008); Per61 is neurotoxic and has been observed in ALS mouse models and human patients, but not in controls (Robertson et al., 2003).

In this study, we show that syncoilin is not limited to muscle and is expressed in the peripheral and central nervous systems. Antibodies generated specifically against Sync1 and Sync2 demonstrate that Sync2 is dominant in the peripheral nervous system and spinal cord whereas Sync1 is dominant in the brain. To determine the function of syncoilin, we show that syncoilin co-localises and interacts with peripherin and also functions to modulate peripherin filament network assembly in vitro. A neuronal assessment of *Sync*$^{-/-}$ mice revealed reactions that were similar to

those of *Sync*$^{+/+}$ mice in a sensory neuron test, but significantly worse than wild-type mice in motor neuron tests. An analysis of spinal cord and dorsal and ventral roots revealed a significant reduction in the number of large-calibre motor axons from the L4-5 region of ventral root motor neurons. The results of this study identify syncoilin as a neuronal IF protein, describe a function for syncoilin, detail a significant neuronal phenotype in the *Sync*$^{-/-}$ mouse and provide a link between syncoilin, peripherin and ALS.

Results

Expression of syncoilin in neuronal tissue

Immunoblots, Q-PCR and immunohistochemistry were performed to determine whether syncoilin is expressed in neurons. Syncoilin was detectable by immunoblot in brain, spinal cord and sciatic nerve using a pan-syncoilin antibody against an N-terminal epitope (anti-syncoilin N-term) (Fig. 1A). Within neurons, spinal cord had the highest relative expression of Sync1 and Sync2, isoforms that are indistinguishable by immunoblot. Detection of Sync3 was visible only in the spinal cord and brain, which are both components of the central nervous system. Antibodies were generated that specifically recognise either Sync1 or Sync2; an antibody against Sync3 was not generated. An immunoblot identically loaded to the one probed for pan-syncoilin was probed for Sync1 and then stripped and re-probed for Sync2. Sync1 was predominantly expressed in the brain, with lower levels in the spinal cord. Sync2 expression was seen in the spinal cord and sciatic nerve. Q-PCR analysis of *Sync1* and *Sync2* mRNA transcript levels reflected the relative protein expression of the two syncoilin isoforms (Fig. 1B). mRNA levels were normalised against GAPDH, and *Sync2* mRNA values were calculated relative to *Sync1* mRNA. In the brain, there was high expression of Sync1 protein and mRNA. *Sync2* mRNA levels were 56% lower than levels of *Sync1* mRNA, and no Sync2 protein was detected by immunoblot. Spinal cord is the only tissue to express both Sync1 and Sync2 protein. Higher Sync2 protein expression was confirmed, with sixfold more *Sync2* mRNA than *Sync1* mRNA. The sciatic nerve exclusively expresses Sync2 protein and had marginally more Sync2 mRNA than *Sync1* mRNA. Sync3 transcripts were detectable by Q-PCR at very low levels that were not of sufficient amplitude to allow for meaningful calculations.

Immunohistochemistry showed syncoilin expression in the sciatic nerve, dorsal root ganglion (DRG) and spinal cord (Fig. 1C). The transverse image of sciatic nerve showed that syncoilin was contained within the axon and not in the surrounding Schwann cells. In the longitudinal image of a sciatic nerve single-teased-fibre preparation, syncoilin localised along the length of the axon and had a punctate appearance around the node of Ranvier in what are probably microvilli. Syncoilin expression was seen in sensory axons and neuron cell bodies of the DRG as well as motor axons and neuron cell bodies of the ventral horn region of the spinal cord.

Co-localisation and interaction of syncoilin and peripherin

Immunohistochemistry analysis was performed in the DRG, spinal cord and sciatic nerve to show that syncoilin co-localised with peripherin (Fig. 2). Extensive but variable overlap of syncoilin and peripherin protein expression exists in neuron cell bodies of the DRG, because expression of one protein in a DRG cell body does not necessarily coincide with strong expression of the other protein. Within the spinal cord, syncoilin was expressed almost exclusively in neuronal cell bodies expressing peripherin, but peripherin was more widely distributed in areas of the spinal cord that did not appear to contain syncoilin. The sciatic nerve, which contains a mixed population of sensory and motor axons, revealed the greatest amount of syncoilin and peripherin co-localisation. This longitudinal view of sciatic nerve demonstrates that syncoilin co-localises with peripherin to the centre of the axon.

Blot-overlay experiments allow for an assessment of syncoilin and peripherin isoform binding. Recombinant syncoilin isoforms Sync1, Sync2 and Sync3, syncoilin domains N-term (residues 1-157; identical in all three isoforms) and rod (residues 158-452; identical in Sync1 and Sync2), and experimental controls maltose-binding protein tag (MBP) and Per58 were used to create two identically loaded protein blots (Fig. 3A). These blots were overlaid with equal amounts of recombinant Per45 or recombinant Per58 and then probed for peripherin under identical conditions. Per45 had strong binding affinity for Sync1, Sync2 and the rod domain with a lesser affinity for Sync3 and N-term syncoilin. Per58 had less binding affinity than Per45 for Sync1, Sync2 and the rod

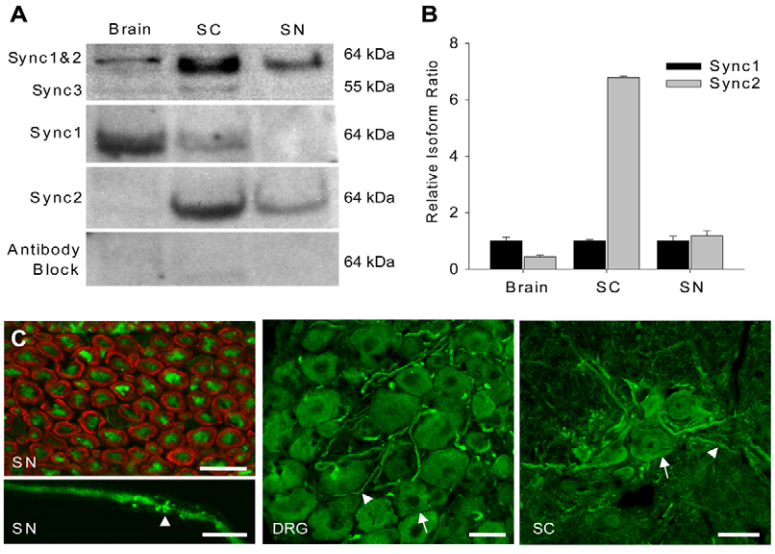

Fig. 1. Syncoilin isoforms are differentially expressed in the nervous system. (**A**) Immunoblots of mouse brain, spinal cord (SC) and sciatic nerve (SN). The top blot probed using a pan-syncoilin antibody (anti-syncoilin N-term) cannot distinguish between Sync1 and Sync2. Below, an identically loaded blot was probed with an antibody specific to Sync1, then stripped and reprobed with an antibody specific to Sync2. An antibody block performed with the Sync1 antibody shows specificity to the isoform-specific peptide antigen and is representative of the blank blot also observed for Sync2. (**B**) Q-PCR of *Sync1* and *Sync2* mRNA transcript levels in brain, spinal cord and sciatic nerve (n=3). *Sync2* mRNA is measured relative to *Sync1* mRNA, which is set to 1. (**C**) Immunohistological analysis of syncoilin (green) expression in transverse (top) and longitudinal (bottom) sciatic nerve, dorsal root ganglion (DRG) and motor neurons of the ventral horn spinal cord. Syncoilin is costained with myelin (red) in the transverse sciatic nerve. The arrowhead in longitudinal sciatic nerve indicates the node of Ranvier. In DRG and spinal cord, arrowheads indicate axons and arrows neuronal cell bodies. Scale bars: 10 μm.

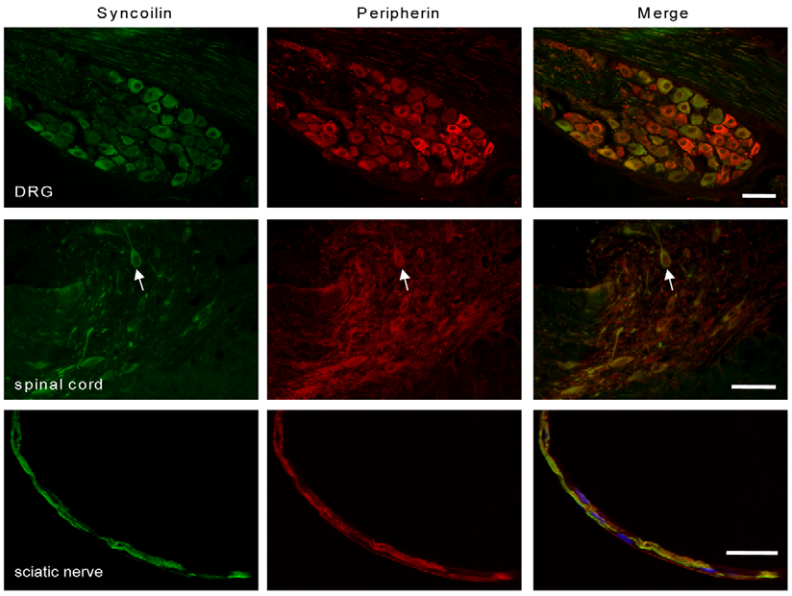

Fig. 2. Syncoilin partially co-localises with peripherin. Syncoilin (green) is costained with peripherin (red) in DRG, motor neurons of the ventral horn of the spinal cord and sciatic nerve. Arrow indicates a spinal-cord cell body. Scale bars: 50 µm (DRG and spinal cord), 20 µm (sciatic nerve).

domain. Per58 also had only weak affinity for Sync3, and no apparent affinity for syncoilin N-term. Neither Per45 nor Per58 interacted with the isolated MBP, confirming the fidelity of the interaction.

Co-immunoprecipitation was used to further demonstrate syncoilin and peripherin binding. Protein lysate from mouse spinal cord was immunoprecipitated with peripherin and syncoilin antibodies (Fig. 3B). Desmin antibody was used as a negative control because desmin is an IF that is not expressed in neurons. One immunoblot probed for syncoilin showed that syncoilin was immunoprecipitated by both peripherin and syncoilin antibodies. The no-antibody and desmin-negative controls were negative for peripherin, demonstrating specificity. The second immunoblot probed for peripherin showed that both Per58 and Per45 co-immunoprecipitated with syncoilin. The no-antibody negative control showed that only very low levels of Per45 and Per58 were non-specifically pulled down by the beads; the desmin-negative control lane showed secondary antibody recognition of the mouse heavy chain IgG.

The role of syncoilin in formation of peripherin filament networks

Given that syncoilin and peripherin co-localised and interacted, experiments were performed to determine whether a functional relationship exists between the proteins. A subclone of the human adrenal cortex carcinoma-derived cell line known as SW13vim(–) lacks all known classes of cytoplasmic IF proteins (Hedberg and Chen, 1986). SW13vim(–) cells transfected with peripherin (both Per45 and Per58) (Fig. 4A), Per45 (Fig. 4C) and Per58 (Fig. 4E) confirm previous reports of formation of peripherin filament networks (McLean et al., 2008). The peripherin filament network of each transfection was blindly graded as 'full', 'partial' or 'none' using parameters of filament length, thickness and arborisation. Transfection of peripherin (*Prph*), the gene that encodes Per58 as well as Per45 via an in-frame downstream initiation codon, typically resulted in a fully formed filament network. When Per45 was transfected alone it formed no filament network, but instead resulted in dense and diffuse cytoplasmic immunostaining. Per58 transfected alone formed a filament network consisting of shorter

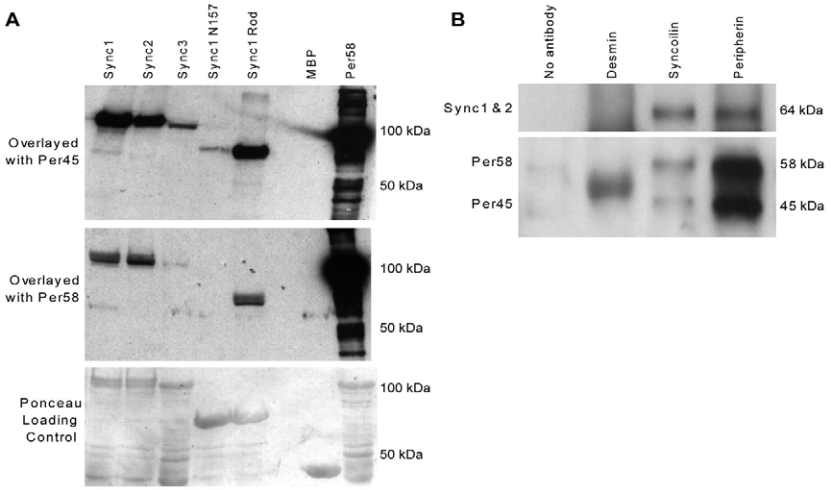

Fig. 3. Syncoilin and peripherin interact. (**A**) Identically loaded immunoblots of recombinant syncoilin isoforms, syncoilin domains and experimental controls were overlaid with equal amounts of either recombinant Per45 or recombinant Per58 and probed under identical conditions for peripherin. A Ponceau-S-stained blot shows equal protein loading and maltose-binding protein and per58 serve as negative and positive controls, respectively. (**B**) Co-immunoprecipitations from mouse spinal cord using rabbit anti-peripherin, anti-syncoilin N-term and anti-desmin antibodies. Immunoblots were probed with anti-syncoilin N-term and mouse anti-peripherin. The no-antibody and desmin co-immunoprecipitations served as negative controls.

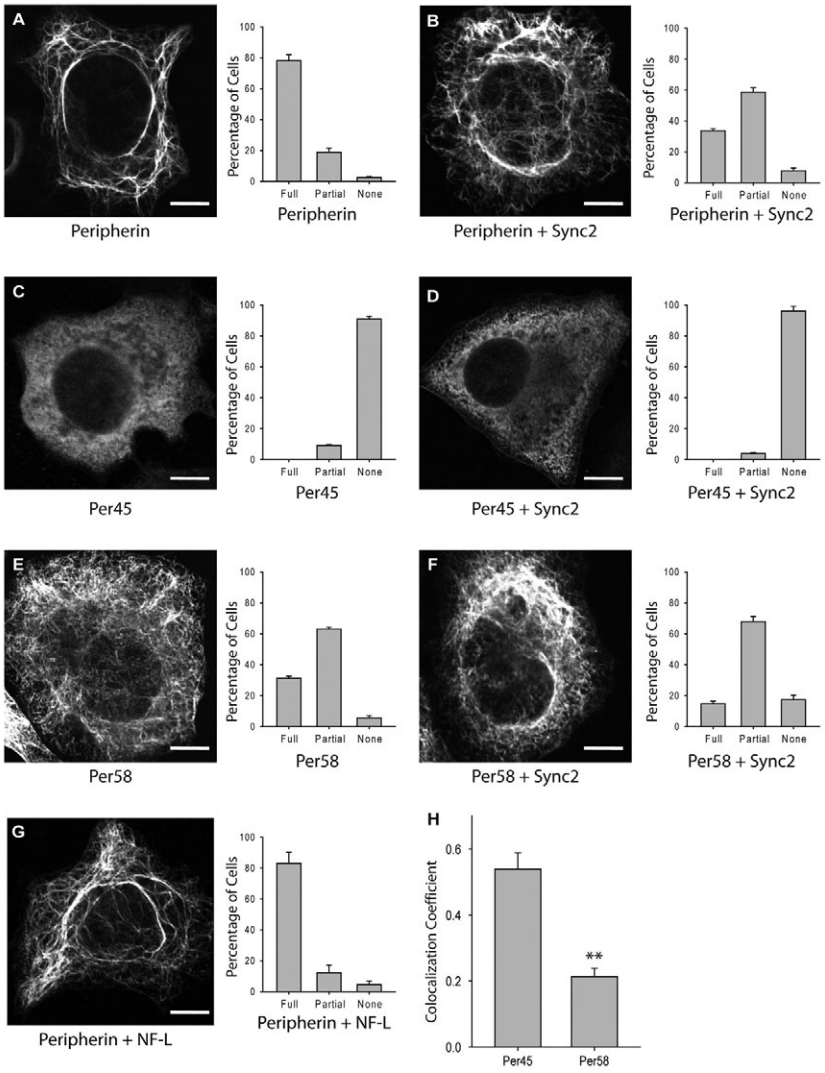

Fig. 4. Syncoilin modulates peripherin filament network formation. (**A-G**) SW13vim(–) cells were singly transfected with peripherin (A), Per45 (C) and Per58 (E). SW13vim(–) cells were co-transfected with Sync2 and peripherin (B), Sync2 and Per45 (D), Sync2 and Per58 (F) and peripherin and NF-L (G). Cells were stained for peripherin. Scale bars: 10 μm. To the right of the representative transfection images is a graph showing the percentage of cells in the three peripherin filament network classifications. 60 cells were counted in each of three separate transfection experiments. The preferential co-localisation of syncoilin with Per45 over Per58 (**H**) was statistically significant (**P<0.001) when analysed using Student's t-test.

and less-organised filaments than the network in *Prph*-transfected cells.

As Sync2 is the dominant syncoilin isoform in spinal cord and sciatic nerve, Sync2 was co-transfected with peripherin (Fig. 4B), Per45 (Fig. 4D) and Per58 (Fig. 4F). Co-transfections of Sync1 with the different peripherin constructs had very similar results (not shown). Peripherin staining in the syncoilin co-transfected cells is noticeably different from staining in cells singly transfected with peripherin. Approximately 78% of *Prph*-transfected cells were categorised as having a full filament network. When Sync2 was co-transfected with peripherin, only 34% of cells had a full filament network, whereas 59% formed a partial filament network and 8% of cells formed no filament network. The difference between peripherin filament networks with and without transfected Sync2 is statistically significant (P<0.05) by ANOVA analysis followed by t-test Bonferroni post-hoc correction. To demonstrate specificity of syncoilin in the modulation of peripherin filament networks, the neuronal IF protein neurofilament-L (NF-L) was co-transfected into SW13 vim(–) cells. Full peripherin filament networks were formed in the presence of other IF proteins. The interaction of syncoilin and peripherin was also studied in the neuronal N2a cell line (supplementary material Fig. S1). Endogenously expressed peripherin formed an IF network whereas endogenous syncoilin expression was diffuse. The overexpression of transfected syncoilin almost completely disrupted the endogenous peripherin network.

Fig. 4D shows Per45 expression when co-transfected with syncoilin to be punctate and diffuse throughout the cytoplasm, which was almost identical to the expression in cells singly transfected with Per45 in Fig. 4C. The Per58 and syncoilin co-transfected cell in Fig. 4F resembles the partial filament network of Per58 transfected alone in Fig. 4E. Cells co-transfected with Sync2 and Per45 or Per58 were analysed for co-localisation (Fig. 4H, images in supplementary material Fig. S2). Sync2 co-localised with both isoforms, because 53.9% of Sync2 staining overlapped with Per45 and 21.3% of Sync2 staining overlapped with Per58. The greater co-localisation of Sync2 with Per45 was statistically significant (P<0.001).

The solubility of peripherin in transfected SW13vim(–) cells was analysed by immunoblot to further understand how the addition of syncoilin affects peripherin filament network formation. In peripherin-transfected cells without syncoilin (Fig. 5A), both Per45 and Per58 were found in the insoluble fraction whereas Per58 was also found in the soluble fraction. These results are similar to previously reported data (McLean et al., 2008). The addition of

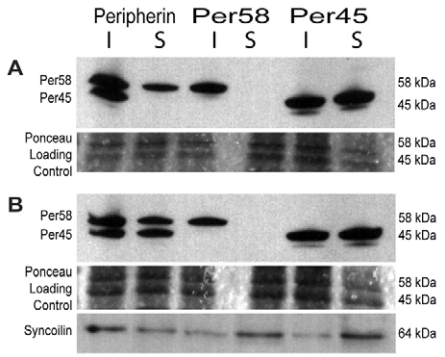

Fig. 5. Syncoilin disrupts the insolubility of Per45 in peripherin-transfected cells. Immunoblots of SW13vim(–) cells transfected with (**A**) Peripherin, Per45 or Per58 and (**B**) Sync2 with peripherin, Per45 or Per58. Cell lysates were fractionated, and the insoluble (I) and soluble (S) fractions were run separately. Ponceau loading controls are shown to verify equal loading. The blot in B was stripped and re-probed for syncoilin to verify the cells were co-transfected.

Sync2 resulted in the solubilisation of some Per45 (Fig. 5B). In cells transfected with only Per58 or Per45, the addition of Sync2 made no difference. Per58 was always found in the insoluble fraction and Per45 was equally split between insoluble and soluble fractions.

Neuronal analysis of *Sync*$^{-/-}$ mice

Since syncoilin expression affects formation of the peripherin filament network and peripherin abnormalities are linked to neuronal disease, a number of experiments were performed to identify a neurological phenotype in the *Sync*$^{-/-}$ mouse. Immunoblots of *Sync*$^{+/+}$ and *Sync*$^{-/-}$ spinal cord and sciatic nerve probed for Per45, Per58 and NF-L demonstrated that the loss of syncoilin has an effect on the expression of Per58 protein but no effect on the expression of Per45 or NF-L protein (Fig. 6A). Four independent repetitions analysed by ImageJ and normalised to β-actin loading controls revealed no difference in Per45 in either tissue or Per58 in sciatic nerve, but did show Per58 levels in spinal cord to be 40% lower in *Sync*$^{-/-}$ mice ($P<0.05$) (Fig. 6B). Since Per45 results from an in-frame downstream start site, individual mRNA isoform analysis could not be achieved. *Prph* (includes Per45 and Per58) mRNA levels in sciatic nerve were unchanged but in spinal cord were 50% lower in *Sync*$^{-/-}$ mice ($P<0.001$) (Fig. 6C).

A standard hotplate test was performed to assess whether *Sync*$^{+/+}$ and *Sync*$^{-/-}$ mice reacted differently to a mild thermal stimulus. The mice were timed from the moment their paws touched the plate until they responded with a hindpaw lick, hindpaw flick or jump. The absence of syncoilin appeared to have no effect on a mouse's pain reflex in response to a thermal stimulus (Fig. 6D). Dorsal roots from the L4-5 region exclusively contain sensory neurons. The loss of syncoilin had no effect on myelinated sensory axon body area (Fig. 6E). The histological appearance of the L4-5 dorsal root showed no overt difference between mice (Fig. 6F).

Several standard motor tests were performed to determine whether *Sync*$^{-/-}$ mice had a motor neuron phenotype. An accelerating rotarod tests both motor coordination and balance. *Sync*$^{+/+}$ mice were able to stay on the rotarod for 266 seconds whereas *Sync*$^{-/-}$ mice averaged only 212 seconds (Fig. 7A). The 20% decline in time spent on the rotarod was found to be statistically significant ($P<0.001$). Given that the accelerating rotarod tests both motor coordination and balance, two experiments

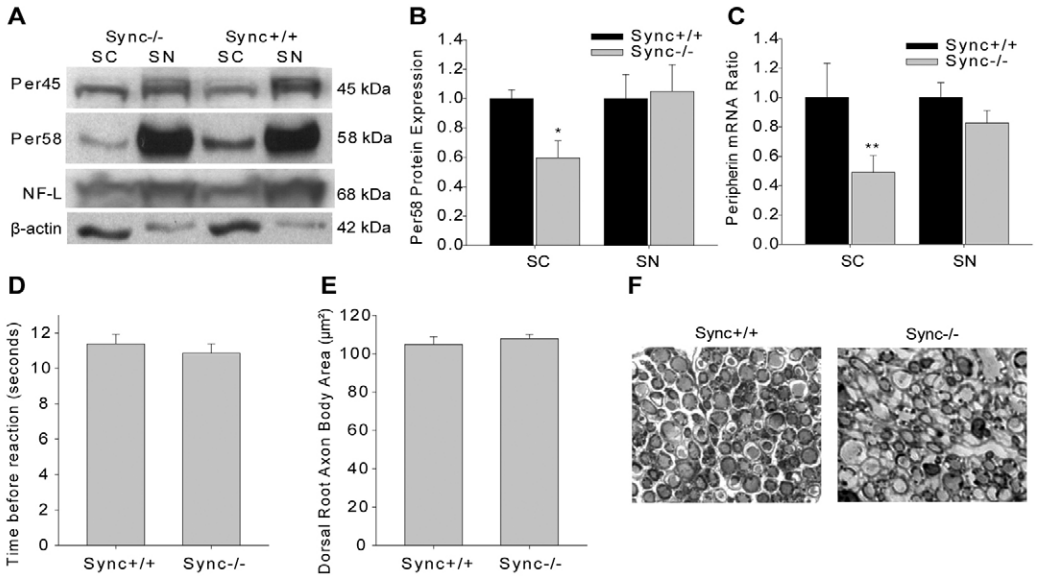

Fig. 6. Per58 is reduced in the *Sync*$^{-/-}$ spinal cord. (**A**) Immunoblot of *Sync*$^{+/+}$ and *Sync*$^{-/-}$ mouse spinal cord (SC) and sciatic nerve (SN) probed for Per45, Per58, neurofilament-L (NF-L) and β-actin loading control. (**B**) Graphical representation of Per58 protein expression in spinal cord and sciatic nerve of *Sync*$^{+/+}$ and *Sync*$^{-/-}$ mice ($n=4$). *Sync*$^{-/-}$ protein levels are measured relative to *Sync*$^{+/+}$ protein, which is set to 1. The reduction of Per58 protein in *Sync*$^{-/-}$ spinal cord was found to be statistically significant (*$P<0.05$) when analysed using Student's *t*-test. No difference was found in Per58 protein levels in sciatic nerve or in Per45 and NF-L protein levels. (**C**) Q-PCR of *Prph* mRNA levels in *Sync*$^{+/+}$ and *Sync*$^{-/-}$ mice in spinal cord and sciatic nerve ($n=3$). *Sync*$^{-/-}$ mRNA is measured relative to *Sync*$^{+/+}$ mRNA, which is set to 1. The reduction of peripherin mRNA in *Sync*$^{-/-}$ spinal cord was found to be statistically significant (**$P<0.001$; Student's *t*-test). (**D**) There was no difference between *Sync*$^{+/+}$ and *Sync*$^{-/-}$ mice in reaction time to a mild thermal stimulus ($n=45$). (**E**) There was no difference in body area of sensory neurons from the dorsal root ($n=5$). (**F**) Representative images of Toluidine-Blue-stained L4-5 dorsal roots.

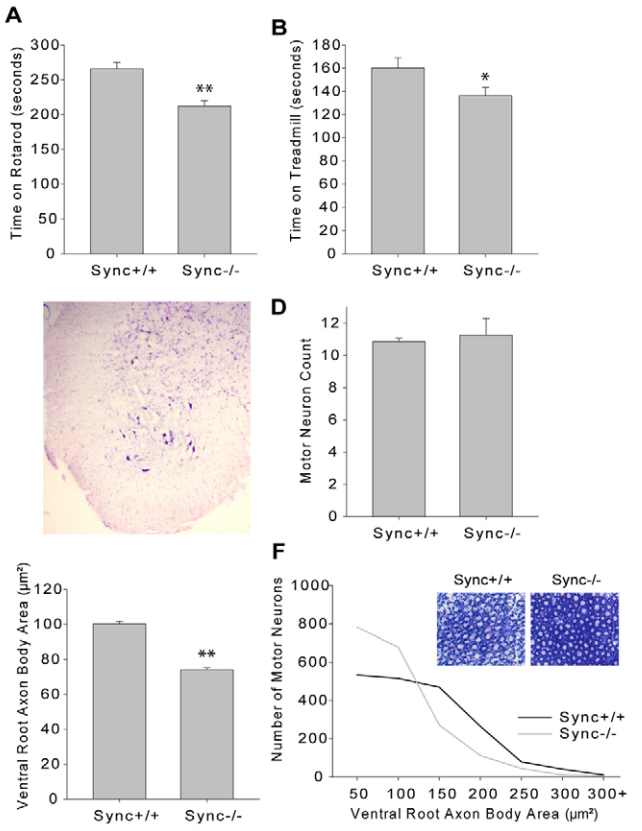

Fig. 7. *Sync*$^{-/-}$ mice perform significantly worse in a range of motor tests and have a decreased motor neuron axon body area when compared with *Sync*$^{+/+}$ mice. (**A**) The decrease in time *Sync*$^{-/-}$ mice were able to remain on an accelerating rotating rotarod was found to be statistically significant (**P<0.001; Student's t-test; n=15). (**B**) The decrease in the time *Sync*$^{-/-}$ mice remained on an accelerating motorised treadmill was found to be statistically significant (*P<0.05; Student's t-test; n=20). (**C**) Representative image of a Cresyl-violet-stained L4-5 spinal cord segment. (**D**) Motor-neuron cell bodies counted from the ventral horn section of *Sync*$^{+/+}$ and *Sync*$^{-/-}$ mice revealed no difference in the number of motor neurons (n=5). (**E**) Areas of motor-neuron axon bodies measured from the L4-5 ventral root revealed a decrease in axon-body area in *Sync*$^{-/-}$ mice that was found to be statistically significant (**P<0.001; Student's t-test; n=8). (**F**) The distribution of areas of ventral-root axon bodies shows that there are more axons with small-body areas and fewer large-body axons in the *Sync*$^{-/-}$ mouse. Included are representative images of *Sync*$^{+/+}$ and *Sync*$^{-/-}$ Toluidine-Blue-stained L4-5 ventral roots.

were performed to further understand the performance difference. Motor coordination and the ability to respond to acceleration were examined using an accelerating treadmill over a short period of time. Mice were timed to see how long they could stay on the treadmill, and *Sync*$^{+/+}$ mice averaged 160 seconds on the treadmill whereas *Sync*$^{-/-}$ mice averaged 136 seconds (Fig. 7B); a statistically significant 14.9% reduction (P<0.05). The second test used to further examine the accelerating rotarod performance difference was the static beam. Balance was assessed as mice were tested for their ability to stay on and walk across a round beam raised above a padded surface. Twenty-six *Sync*$^{+/+}$ and 28 *Sync*$^{-/-}$ mice were tested once; none of the mice fell off the beam. Furthermore, 15 *Sync*$^{+/+}$ mice and 16 *Sync*$^{-/-}$ mice completed the task of walking across the beam, suggesting that the absence of syncoilin has no effect on a mouse's ability to complete this task.

Spinal cord sections from the L4-5 region of the lumbar spinal cord were stained with Cresyl Violet to identify ventral horn motor neurons. Motor neurons were identified as dark, large and irregularly shaped cells in the ventral horn (Fig. 7C). Counts of ventral horn motor neurons in *Sync*$^{-/-}$ mice were comparable with those of normal mice (Fig. 7D). L4-5 ventral roots exclusively contain motor axons. The average axon body area for the *Sync*$^{+/+}$ mouse was found to be 100.2 µm^2 versus 74.2 µm^2 for the *Sync*$^{-/-}$ mouse (P<0.001) (Fig. 7E). A plot of individual axon body areas illustrates a shift of medium to large axons seen in the *Sync*$^{+/+}$ mouse to smaller axons seen more commonly in the *Sync*$^{-/-}$ mouse (Fig. 7F).

Discussion

IFs, microtubules and microfilaments are the three intracellular cytoskeletal structures that provide eukaryotic cells with structure and shape. Here, we show that syncoilin, similarly to the IF proteins, neurofilaments, synemins, peripherins and α-internexin, is expressed in neurons. The creation of two new antibodies allowed for the first analysis of protein expression of the syncoilin isoforms Sync1 and Sync2. Immunoblots of protein levels from brain, spinal cord and sciatic nerve corroborate a Q-PCR analysis of syncoilin isoform RNA transcript levels. In the brain, as in muscle, Sync1 is the dominant syncoilin isoform. Interestingly, Sync2 is the dominant syncoilin isoform in spinal cord and sciatic nerve. These findings are of interest because variable isoform expression in discrete regions of the nervous system suggests that Sync1 and Sync2 might serve different functions both within the nervous system and between muscle and neuronal cells. Sync3 expression is observed only in the brain and spinal cord, both components of the central nervous system. Sync3 is also selectively expressed in certain types of muscle including cardiac muscle and the skeletal muscle soleus that is largely populated by slow (type I) myofibres (McCullagh et al., 2008). Syncoilin is unlike neuronal IF proteins peripherin and neurofilament, whose isoforms are expressed in the same cell types (Lee et al., 1993; McLean et al., 2008). Instead, the different expressions and potentially different functions of the syncoilin isoforms resemble those of the synemin isoforms, two of which are expressed in glial cells during development and one of which is expressed in mature neurons (Izmiryan et al., 2006; Izmiryan et al., 2008).

Syncoilin binds the type III muscle-specific IF desmin in skeletal muscle (Costa et al., 2004). In addition to syncoilin, the only other type III IF protein expressed in neurons is peripherin. It was hypothesised that because desmin and peripherin share features of type III IF proteins, syncoilin and peripherin might interact in neurons. Syncoilin and peripherin are shown in this study to bind by blot overlay and co-immunoprecipitation.

The DRG contains sensory cell bodies whose axons extend to both the dendrites in the periphery and the spinal cord. Within the DRG, syncoilin appeared to have variable but ubiquitous expression in nearly every cell body and to be partially co-localised with peripherin. Syncoilin expression was also seen in the axons of sensory neurons that connect to the DRG cell bodies. Motor neuron cell bodies are found in the ventral horn of the spinal cord and can be easily identified by their shape and location. Syncoilin expression in the spinal cord was restricted to neuronal cells. Peripherin appeared to have a wider expression pattern but always co-localises with syncoilin.

In a single-teased-fibre preparation of sciatic nerve, syncoilin and peripherin were co-localised within the axon but not in

surrounding Schwann cells. Syncoilin expression was punctate in the vicinity of the nodes of Ranvier in what are likely to be microvilli, because the staining extends beyond axonal syncoilin labelling. The nodes of Ranvier are gaps between myelin sheaths that contain protein complexes including voltage-gated Na^+ channels, Na^+/K^+ ATPases, and Na^+/Ca^{2+} exchangers that assist in the propagation of action potentials along myelinated nerve fibres (Susuki and Rasband, 2008). In muscle, syncoilin expression is enriched at the neuromuscular junction (Newey et al., 2001), and many morphological and molecular similarities exist between nodes of Ranvier and neuromuscular junctions (Caldwell, 2000; Ellisman, 1979). Several proteins including N-cadherin (Cifuentes-Diaz et al., 1994), N-CAM and cytotactin (Rieger et al., 1986) are expressed or enriched at both the neuromuscular junction and node of Ranvier and function in cell-cell adhesion, neurite outgrowth and synaptic plasticity. It is unknown why the syncoilin expression pattern changes at the node of Ranvier, but it is possible that syncoilin is involved with one of these functions or interacts with any of the protein complexes at the node.

Upon transfection in SW13vim(–) cells lacking an IF network, peripherin (Per45+Per58) forms a full IF network. Alone, Per58 is capable of forming a partially disrupted network, but Per45 alone forms no network. Syncoilin transfected into SW13vim(–) cells was incapable of forming an IF network. The addition of Sync2 to peripherin resulted in a partially disrupted peripherin network that resembled the Per58 partially disrupted filament network. This suggests that the addition of Sync2 to a peripherin-transfected cell has the same effect as the removal of Per45 from a peripherin-transfected cell. In a solubility assay of transfected SW13vim(–) cell protein lysates, filament network-forming peripherin (Per45 + Per58) was found largely in the insoluble fraction although a portion of Per58 was found in the soluble fraction. This is puzzling because Per58 alone is entirely insoluble. The presence of Per45 is therefore able to solubilise a portion of the Per58 isoform from the insoluble filament structures, possibly reflecting the role of Per45 in regulating peripherin filament networks. More importantly, the addition of Sync2 to a peripherin-transfected cell resulted in the relocation of some Per45 from the insoluble to the soluble fraction. The Sync2-dependent redistribution of some Per45 from the insoluble to the soluble fraction is a likely explanation for the partial disruption of peripherin filament networks. It is possible that Sync2 disrupts the peripherin filament network by sequestering Per45 away from peripherin. This hypothesis is further supported by the fact that the addition of Sync2 to Per58 in transfected cells appeared to have no affect on the solubility of Per58 and no further impact on the already partially disrupted Per58 network. Furthermore, Sync2 exhibited preferential co-localisation with Per45 over Per58 in transfected cells. Since Per45 is necessary for full formation of filament networks, it is possible that Sync2 acts to modulate peripherin filament network formation. Syncoilin could actively sequester and release Per45, thereby controlling the growth and maintenance of the peripherin IF network in response to further cellular stimuli.

Several neuronal IF proteins are associated with human disease. Peripherin and the neurofilaments are often found in inclusion bodies in motor neurons of patients with the disease ALS (Al-Chalabi et al., 1999; Figlewicz et al., 1994; Mitchell and Borasio, 2007; Xiao et al., 2006; Kemp and Davies, 2007). It was first determined whether the loss of syncoilin had an effect on any other neuronal IF proteins. NF-L is essential for the assembly of neurofilaments and serves as an indicator of normal neuronal structures (Zhu et al., 1997). NF-L and peripherin protein levels were analysed by immunoblot. NF-L was unchanged in spinal cord and sciatic nerve in the *Sync*$^{-/-}$ mouse, suggesting that syncoilin is not essential for neurofilament expression and stability. Also unchanged were Per45 protein levels in spinal cord and sciatic nerve as well as Per58 protein and *Prph* (Per45+Per58) mRNA levels in sciatic nerve. However, Per58 protein and *Prph* mRNA levels were significantly reduced in the spinal cord. If syncoilin acts to modulate peripherin filament network assembly, it is possible that peripherin filament networks, which consist primarily of Per58, are unstable and then degraded in the absence of syncoilin. However, it remains unknown why Per58 levels are affected only in the spinal cord or why Per45 is not reduced in the spinal cord with Per58. This could be due to the differences between spinal cord and sciatic nerve syncoilin isoform expression, neuron structure or neuron function.

Given the range of phenotypes from IF transgenic and knockout mice and the minimal muscle phenotype in the *Sync*$^{-/-}$ mouse, the *Sync*$^{-/-}$ mouse was examined in a wide range of sensory and motor neuron tests. The hotplate test is an established method for testing the response to a thermal stimulus (Gu et al., 2002). The fact that there was no difference in hotplate-response time between *Sync*$^{+/+}$ and *Sync*$^{-/-}$ mice suggests that syncoilin is not essential for nociception – the neural processing in the central and peripheral nervous system of painful stimuli. An analysis of sensory neurons from the dorsal root also revealed no difference between *Sync*$^{+/+}$ and *Sync*$^{-/-}$ axon-body area. This is interesting because the loss of peripherin results in a substantial reduction in the number of L5 unmyelinated sensory fibres (Lariviere et al., 2002). Unfortunately, owing to Home Office regulations, no further relevant sensory neuron tests could be performed.

We also performed several motor-neuron-specific tests. Most of these tests could also assess muscle function. However, voluntary and extended forced running tests and extensive histological analyses revealed minimal muscular differences between *Sync*$^{+/+}$ and *Sync*$^{-/-}$ mice (McCullagh et al., 2008). Therefore, it is possible that any motor phenotype discovered in the *Sync*$^{-/-}$ mouse is the result of a neuronal change. An accelerating rotarod requires motor coordination and balance (Dunham and Miya, 1957). This test demonstrated the most significant difference between *Sync*$^{+/+}$ and *Sync*$^{-/-}$ mice, confirmed a neuromuscular deficiency in the *Sync*$^{-/-}$ mouse and introduced possible defects including balance and coordination. The accelerating treadmill test is designed to examine the ability of a mouse in a rapidly accelerating environment akin to a sprint. This treadmill test differs from the rotarod because it does not require the same degree of balance or coordination needed to stay on the apparatus. A previous study of forced treadmill running at constant speeds was designed to run the mice to exhaustion but revealed no difference between *Sync*$^{+/+}$ and *Sync*$^{-/-}$ mice (McCullagh et al., 2008). *Sync*$^{-/-}$ mice performed significantly worse than *Sync*$^{+/+}$ mice in the accelerating treadmill test. EDL is a fast glycolytic tissue containing approximately 77% type IIb fibres that are primarily used for activities such as sprinting (Nemeth and Pette, 1980). An analysis of EDL muscle in the *Sync*$^{-/-}$ mouse found a 27.9% reduction in force generation (McCullagh et al., 2008). It is probable that the defect in EDL muscle contributes to the reduced ability of *Sync*$^{-/-}$ mice in these tests. To specifically examine balance, a factor in the accelerating-rotarod test, a standard static-beam test was used (Le Marec et al., 1997). The ability of *Sync*$^{-/-}$ mice to stay on the beam, turn and to walk to the

end of the beam at the same frequency of *Sync*$^{+/+}$ mice suggests that syncoilin is not essential for proper balance or coordination.

Taken together, the range of behavioural tests suggests a neuromuscular deficiency in *Sync*$^{-/-}$ mice. Two histological examinations of the quantity and quality of motor neurons were performed in an effort to find a cause for the neuromuscular phenotype. An examination of motor neurons in the ventral horn of the lumbar spinal cord in *Sync*$^{+/+}$ and *Sync*$^{-/-}$ mice revealed that the loss of syncoilin does not affect the quantity of motor neurons. Motor neurons from the L4-5 region are known to innervate muscles of the lower limb such as EDL (Tyc and Vrbova, 2007). Ventral roots from the L4-5 region were used to exclusively examine the quality of motor neurons. No obvious histological difference were seen, but motor neuron axon body area was measured and found to be significantly smaller in the *Sync*$^{-/-}$ mouse, which is possibly an indication of reduced neuronal transmission. It is also possible that syncoilin functions independently or via some other unknown mechanism to regulate the diameter of large-calibre axons (Hirokawa, 1982). Although *Sync*$^{-/-}$ mice have no overt phenotype throughout their lifetimes, moderate neuronal deficiencies caused by the absence of syncoilin might contribute to a reduced neuromuscular ability. In the accelerating-rotarod and accelerating-treadmill tests, *Sync*$^{-/-}$ were always able to complete the tasks; instead, the difference between *Sync*$^{+/+}$ and *Sync*$^{-/-}$ mice was how well the task was completed. This distinction fits well with the observed histological phenotype of motor neurons in *Sync*$^{-/-}$ mice. The absence of syncoilin does not result in the loss of motor neurons. Instead, it is hypothesised that the loss of syncoilin results in a shift of large-calibre to small-calibre axons with a reduced ability to transmit neurological signals to muscles. We hypothesise that the reduction in large-calibre motor neurons in the L4-5 region inhibits full EDL function during accelerating tasks such as the rotarod and treadmill, and results in the reduction in force generation previously described (McCullagh et al., 2008; Zhang et al., 2008). This suggests that EDL muscle has undergone an inherent change in its muscle contractile characteristics owing to a chronic lack of proper neural transmission. The specific impairment of EDL function can be explained by the Henneman size principle, which states large-calibre motor neurons preferentially innervate type IIb fibres that are abundant in EDL muscle (Henneman, 1957).

In conclusion, we found that the IF protein syncoilin is expressed in neurons and that it interacts with peripherin isoforms. The loss of syncoilin results in a significant neuronal phenotype, and we show that syncoilin might mediate assembly of peripherin filament networks by interacting with Per45. Previous studies have implicated syncoilin in muscle disease. The findings of this study raise the potential for the involvement of syncoilin in diseases associated with neuronal IFs. In particular, the association of peripherin with ALS and the ability of syncoilin to alter assembly of peripherin filament networks introduces the possibility of the involvement of syncoilin in this disease.

Materials and Methods

Animals and antibodies

Syncoilin null (*Sync*$^{-/-}$) and wild type (*Sync*$^{+/+}$) mice were generated and bred in-house as described previously (McCullagh et al., 2008). All experimental procedures involving the use of animals were performed in accordance with guidelines approved by the Home Office. All experiments were performed with 6- to 8-week-old mice. Antibodies used include rabbit anti-Sync-N-term (Newey et al., 2001), mouse anti-desmin (Abcam 8592), mouse anti-peripherin (Chemicon MAB5380), rabbit anti-peripherin (Chemicon MAB 1530), chicken anti-peripherin (Chemicon AB9282), rabbit anti-NF-L (Abcam 9035), mouse anti-myelin basic protein (Dytrych et al., 1998), goat anti-α-actinin (Santa Cruz N-19) and Alexa Fluor 594- and Alexa Fluor 488-conjugated IgG secondary antibodies (Invitrogen). Newly described rabbit polyclonal antibodies anti-Sync1 and anti-Sync2 were generated by Eurogentec from the Keyhole limpet haemocyanin-coupled peptide antigens H_2N-CTSQAGGVEAQSPGTV-COOH and H_2N-CSPETRKHLLKDH-COOH, respectively.

Histology and immunofluorescence

Mice were perfused with 2% paraformaldehyde in a phosphate buffer (25 mM NaH_2P0_4, 8 mM Na_2HPO_4). Tissues were dissected, post-fixed in 4% paraformaldehyde and cryoprotected in 30% sucrose solution. For motor neuron counts of the spinal cord ventral horn, 10 μm sections were stained with 0.5% Cresyl Violet (Sigma), washed in a H_2O and alcohol series, cleaned with Histochoice Clearing Agent (Sigma) and mounted with Histomount (RA Lamb). Dorsal and ventral roots were dissected from the L4-L5 region of the spinal cord in perfused mice and stored in 70% ethanol until embedding, sectioning and staining were done by Mohan Masih (DPAG, University of Oxford, Oxford, UK). Dorsal-ventral roots were embedded in Araldite resin, sectioned at a thickness of 1 μm and stained with a solution of 1% Toluidine Blue and 1% borax.

Tissue for immunofluorescence was perfused, fixed and cryoprotected as above. Tissue was embedded in OCT (BDH), sectioned on a cryostat to a thickness of 10 μm. Teased fibre preparations from fixed isolated sciatic nerve were perfused and cryoprotected as described above and teased using fine instruments in PBS on 3-aminopropyltriethoxysilane (TESPA)-coated slides. All immunofluorescence samples were blocked for 1 hour in 10% fetal calf serum in PBS. Primary antibodies as described above were diluted in blocking solution and applied to fixed sections for 1 hour. Sections were rinsed in PBS and incubated with secondary antibodies described above in blocking solution for 1 hour. Finally, sections were rinsed thoroughly and mounted in Vectashield aqueous medium with DAPI (National Diagnostic).

All microscope work was performed at room temperature. Co-localisation images were taken using a 510 Meta confocal laser-scanning microscope and analysed using LSM Image 4.0 software. All parameters [(63×/1.4 oil DIC objective), zoom (2), averaging (4)] were kept equal and images were adjusted so no saturation occurred and background was slightly above zero. Whole cells were selected as regions of interest (ROIs) and threshold was set from the ROIs. Other imaging was performed with an AxioPlan microscope, AxioCam HRc and Axiovision LE 4.6 software. Plan-neofluar 10×/0.3, 20×/0.5, 40×/0.75 objective lenses were used in both microscopes (all imaging products from Carl Zeiss). Axon calibre was measured blindly using Axiovision by outlining individual axons. Classification of peripherin filament networks was determined using three parameters: length, thickness of filaments and arborisation. Full networks contained long, continuous filament bundles with extensive arborisation and minimal punctate spots. Partial networks contained shorter filaments or thick bundles with little arborisation and significant punctate staining. Cells classified as having no filament network contained no evidence of filament formation and only punctate expression. Counts were performed blindly on 60 cells of each transfection during three different experiments for a total of 180 cells.

Protein and RNA preparation

Tissue from *Sync*$^{+/+}$ and *Sync*$^{-/-}$ mice was homogenised in an appropriate volume of cold Newcastle buffer (75 mM Tris-HCl, pH 6.8, 3.8% SDS, 4 M urea and 20% glycerol) with protease inhibitor cocktail (Sigma). Protein quantification was performed with the Bio-Rad DC Protein assay according to the manufacturer's protocol. For total RNA extraction, dissected tissue was snap frozen and milled in liquid nitrogen immediately before using Trizol (Invitrogen) according to the manufacturer's instructions. Total RNA (300 ng) was reverse transcribed into cDNA using random decameric primers and SuperScript II Reverse Transcriptase (Invitrogen). Generated cDNA was used as a template to perform PCR analysis. The solubility assay protocol was adapted from published techniques (McLean et al., 2008). Briefly, cells were harvested in low-salt lysate buffer [20 mM Tris-HCl, pH 7.5, 150 mM NaCl, 1 mM EDTA, 1% (v/v) Triton X-100 and protease inhibitors (all from Sigma)], briefly homogenised and incubated on ice for 30 minutes. The lysates were centrifuged at 16,000 ***g*** for 30 minutes at 4°C to separate soluble and insoluble fractions. The insoluble fraction was solubilised in 2% (w/v) SDS in lysate buffer and made up to a volume equal to the soluble fraction. Samples were concentrated equally in a Centriplus filter device (Millipore) according to the manufacturer's instructions. Equal volumes of each fraction were run on a gel and immunoblotted as described below.

Immunoblotting

80 μg total protein from tissue lysates was separated on 8% SDS polyacrylamide gels (Bio-Rad) and electrophoretically transferred to nitrocellulose membranes. After blocking membranes for 1 hour in TBS-T [Tris-buffered saline containing 0.1% (v/v) Tween 20] and 5% nonfat dry milk, blots were incubated overnight with primary antibody in blocking buffer and washed three times in TBS-T before incubation for 1 hour with horseradish-peroxidase-conjugated IgG secondary antibody (GE) in blocking buffer. Membranes were washed and developed using ECL detection reagents (GE) according to the manufacturer's instructions. Blots were stripped at

50°C for 20 minutes in stripping buffer (100 mM 2 mercaptoethanol, 2% SDS, 62.5 mM Tris-HCl) before re-probing with different antibodies. Exposed film was scanned with a HP Scanjet 5400c. Protein expression was measured from immunoblot intensity using ImageJ (Abramoff et al., 2004).

Blot-overlay analysis

Using standard cloning techniques and endonuclease (5′, EcoRI; 3′, *Hin*dIII) sequence-tagged primers, Sync1-Sync3, Per45 and Per58 were subcloned from pcDNA3 into pMAL (New England Biolabs) using standard methodologies. Syncoilin N-term (residues 1-157) and rod domains (residues 158-452) were subcloned into pMAL using the following primers: N-termF, TTT GAA TTC ATG GCC AGC CCG GAA CCC CT; N-termR, TTT AAG CTT AGA GGG GAT CCT CCT CGG TGT; RodF, TTT GAA TTC AGC GTG GAG GAC CTG GAG CG; RodR, TTT AAG CTT ATG CAT CAG CCT GTT CCA GAC. Expression and purification of maltose-binding protein (MPB)-tagged proteins were performed using the pMAL protein fusion and purification system, in accordance with the manufacturer's instructions (New England Biolabs). 10 µg MBP-tagged recombinant proteins were separated on gels and transferred to nitrocellulose membranes as described above. Membranes were blocked for 1 hour and incubated with 5 ml MBP-tagged Per45 or Per58 (3 µg/ml) in blocking buffer for 2 hours. Membranes were washed, probed with mouse anti-peripherin antibody and then treated as described above.

Co-immunoprecipitation

Spinal-cord tissue was crushed in liquid nitrogen and then added to immunoprecipitation lysis buffer with CHAPS, which partially solubilises syncoilin and peripherin (50 mM Tris-HCl, pH 7.5, 150 mM NaCl, 1% w/v CHAPS, 1% v/v protease inhibitor cocktail). Samples were homogenised, lysed on ice, centrifuged at 13,000 ***g*** for 10 minutes at 4°C and supernatants removed. Lysate supernatants were pre-cleared by rotating with 20 µl Protein-G-Sepharose beads for 2 hours at 4°C. Pre-cleared beads were removed, and 5 µg antibody was added to samples and incubated rotating overnight at 4°C. 30 µl of pre-equilibrated Protein-G-Sepharose beads were added to each sample and rotated at 4°C for 2 hours. Beads were washed three times with 1 ml lysis buffer without CHAPS and proteins were eluted by boiling in 1× NuPAGE LDS sample buffer (Invitrogen) with β-mercaptoethanol for 2 minutes. Supernatants were used for immunoblotting as described above.

Quantitative PCR

Q-PCR analysis of Sync1, Sync2 and peripherin was performed on an ABI Prism 7000 using 2× power SYBR master mix (ABI) in a total volume of 20 µl. Measured fluorescence was normalised against GAPDH. Syncoilin primers were designed to take advantage of unique exon boundaries created by the syncoilin splice isoforms. Primers used were: Sync1F, CAAAAACGCGATGAAGAGGT, Sync1R, GGGTA-GCATAGCCTTATATGTGGA; Sync2F, CAAAAACGCGATGAAGAGGT, Sync2R, TCTAAACAGTCCTTATATGTGGAAAGC; PeripherinF, AGCTACTGGAAGG-GGAGGAG, PeripherinR, CGGGTCTCAATTGTCCTGAT; GAPDH-F, ACTCC-ACTCACGGCAAATTC, GAPDH-R, TCTCCATGGTGGTGAAGACA. Three age- and sex-matched adult animals from each genotype were used for each transcript analysis and all reactions were performed in triplicate. Data was exported using SDS1.2.3 from ABI. Reaction efficiency was calculated for each primer pair using averaged kinetic data obtained from at least 50 individual reactions (Tichopad et al., 2003). Data were processed using a method described by Funke-Kaiser and co-workers (Schefe et al., 2006).

Cell Culture

SW-13vim(–) cells were seeded on uncoated coverslips in 12-well plates. After 24 hours, they were transfected with 0.5 µg DNA per well using FuGENE (Roche) at a ratio of 1 µg DNA to 3 µl FuGENE following the manufacturer's protocol. Cells were cultured for 48 hours before being fixed and permeabilised for 20 minutes in cold methanol at –20°C and immunostained as described above. Syncoilin isoform constructs were used as previously described (Kemp et al., 2008). Peripherin expression vectors were kind gifts from Jean-Pierre Julien (Université Laval, Quebec, Canada) and Janice Robertson (University of Toronto, Canada). The Per45 and Per58 constructs were generated as described (McLean et al., 2008). NF-L construct was created using primers NF-L F, GCACCGGCCGCCACCATGAGT, NF-L R, GTTGGGAATAGGGCTCAATG. PCR products were cloned into pCDNA3 with 5′ *Eco*RI and 3′ *Not*I adapters. All transfection data expressed as mean ± s.e.m., multiple statistical comparison between groups was performed by ANOVA test, with Bonferroni's *t*-test post-hoc correction for a better evaluation of intra-group and inter-group variability and avoiding false positives (De Luca et al., 2003; De Luca et al., 2005).The source of all cDNA used in this paper was mouse. N2a cells were cultured in MEM + Earle's, 1% non-essential amino acids (NEAA), 10% foetal calf serum (FCS), 2 mM glutamine, 100 U/ml penicillin and 0.1 mg/ml streptomycin and were passaged approximately 1:5 twice a week.

Behavioural testing

The rotarod device consists of a mechanically controlled grooved plastic beam 5 cm in diameter (Ugo Basile, Italy). Mice were placed on the beam rotating initially at a speed of 5 rotations per minute. Rod speed was gradually accelerated to a maximum of 40 rotations per minute over 5 minutes. Fifteen 2-month-old mice of each genotype were tested for their ability to stay on the rod and were tested four times each on separate days.

Mice were placed on a 55°C hotplate surrounded by a clear acrylic cage. Mice were timed from the moment they were put on the hotplate until the observation of a physical response identified by hindpaw lick, hindpaw flick or jump. Forty-five 2-month-old mice of each genotype were allowed to stay on the hotplate for a maximum of 30 seconds and were tested only once.

Mice were placed on a motorised treadmill (Exer6-M, Columbus Instruments) initially at a speed of 5 m/minute. The treadmill speed was gradually accelerated to a maximum of 30 m/minute over 5 minutes. Twenty-two-month-old mice of each genotype were tested for their ability to stay on the treadmill. Mice were tested only once.

A wooden dowel 28 mm diameter and 60 cm in length was clamped to a bench 60 cm above a padded surface. Mice were placed on the protruding end of the rod facing away from the bench. The time taken to reach the end of the beam attached to the bench or fall from the rod was recorded up to a maximum of 3 minutes. Twenty-six $Sync^{+/+}$ and 28 $Sync^{-/-}$ 2-month-old mice were tested only once.

This work was funded by the Medical Research Council, Muscular Dystrophy Association USA and Association Française Contre les Myopathies. W.T.C. was funded by a Marshall Scholarship. The authors are grateful to Mohan Masih, Dirk Baumer, Simon D'Alton and Peter Oliver (all Department of Physiology, Anatomy and Genetics, University of Oxford) for technical assistance, University of Oxford Biomedical Services staff for animal husbandry and Jean-Pierre Julien (Université Laval, Quebec, Canada) and Janice Robertson (University of Toronto, Canada) for kindly providing peripherin expression vectors. Deposited in PMC for release after 6 months. This article is freely accessible online from the date of publication.

Supplementary material available online at
http://jcs.biologists.org/cgi/content/full/123/15/2543/DC1

References

Abramoff, M. D., Magelhaes, P. J. and Ram, S. J. (2004). Image processing with ImageJ. *Biophotonics International* **11**, 36-42.

Al-Chalabi, A., Andersen, P. M., Nilsson, P., Chioza, B., Andersson, J. L., Russ, C., Shaw, C. E., Powell, J. F. and Leigh, P. N. (1999). Deletions of the heavy neurofilament subunit tail in amyotrophic lateral sclerosis. *Hum. Mol. Genet.* **8**, 157-164.

Brown, S. C., Torelli, S., Ugo, I., De Biasia, F., Howman, E. V., Poon, E., Britton, J., Davies, K. E. and Muntoni, F. (2005). Syncoilin upregulation in muscle of patients with neuromuscular disease. *Muscle Nerve* **32**, 715-725.

Caldwell, J. H. (2000). Clustering of sodium channels at the neuromuscular junction. *Microsc. Res. Tech.* **49**, 84-89.

Cifuentes-Diaz, C., Nicolet, M., Goudou, D., Rieger, F. and Mege, R. M. (1994). N-cadherin expression in developing, adult and denervated chicken neuromuscular system: accumulations at both the neuromuscular junction and the node of ranvier. *Development* **120**, 1-11.

Costa, M. L., Escaleira, R., Cataldo, A., Oliveira, F. and Mermelstein, C. S. (2004). Desmin: molecular interactions and putative functions of the muscle intermediate filament protein. *Braz. J. Med. Biol. Res.* **37**, 1819-1830.

De Luca, A., Pierno, S., Liantonio, A., Cetrone, M., Camerino, C., Fraysse, B., Mirabella, M., Servidei, S., Ruegg, U. T. and Conte Camerino, D. (2003). Enhanced dystrophic progression in mdx mice by exercise and beneficial effects of taurine and insulin-like growth factor-1. *J. Pharmacol. Exp. Ther.* **304**, 453-463.

De Luca, A., Nico, B., Liantonio, A., Didonna, M. P., Fraysse, B., Pierno, S., Burdi, R., Mangieri, D., Rolland, J. F., Camerino, C. et al. (2005). A multidisciplinary evaluation of the effectiveness of cyclosporine a in dystrophic mdx mice. *Am. J. Pathol.* **166**, 477-489.

Dunham, N. W. and Miya, T. S. (1957). A note on a simple apparatus for detecting neurological deficit in rats and mice. *J. Am. Pharm. Assoc. Am. Pharm. Assoc. (Baltim)* **46**, 208-209.

Dytrych, L., Sherman, D. L., Gillespie, C. S. and Brophy, P. J. (1998). Two PDZ domain proteins encoded by the murine periaxin gene are the result of alternative intron retention and are differentially targeted in schwann cells. *J. Biol. Chem.* **273**, 5794-5800.

Ellisman, M. H. (1979). Molecular specializations of the axon membrane at nodes of ranvier are not dependent upon myelination. *J. Neurocytol.* **8**, 719-735.

Figlewicz, D. A., Krizus, A., Martinoli, M. G., Meininger, V., Dib, M., Rouleau, G. A. and Julien, J. P. (1994). Variants of the heavy neurofilament subunit are associated with the development of amyotrophic lateral sclerosis. *Hum. Mol. Genet.* **3**, 1757-1761.

Grady, R. M., Grange, R. W., Lau, K. S., Maimone, M. M., Nichol, M. C., Stull, J. T. and Sanes, J. R. (1999). Role for alpha-dystrobrevin in the pathogenesis of dystrophin-dependent muscular dystrophies. *Nat. Cell Biol.* **1**, 215-220.

Gu, Y., McIlwain, K. L., Weeber, E. J., Yamagata, T., Xu, B., Antalffy, B. A., Reyes, C., Yuva-Paylor, L., Armstrong, D., Zoghbi, H. et al. (2002). Impaired conditioned fear and enhanced long-term potentiation in Fmr2 knock-out mice. *J. Neurosci.* **22**, 2753-2763.

Hedberg, K. K. and Chen, L. B. (1986). Absence of intermediate filaments in a human adrenal cortex carcinoma-derived cell line. *Exp. Cell Res.* **163**, 509-517.
Henneman, E. (1957). Relation between size of neurons and their susceptibility to discharge. *Science* **126**, 1345-1347.
Hirokawa, N. (1982). Cross-linker system between neurofilaments, microtubules, and membranous organelles in frog axons revealed by the quick-freeze, deep-etching method. *J. Cell Biol.* **94**, 129-142.
Izmiryan, A., Cheraud, Y., Khanamiryan, L., Leterrier, J. F., Federici, T., Peltekian, E., Moura-Neto, V., Paulin, D., Li, Z. and Xue, Z. G. (2006). Different expression of synemin isoforms in glia and neurons during nervous system development. *Glia* **54**, 204-213.
Izmiryan, A., Franco, C. A., Paulin, D., Li, Z. and Xue, Z. (2008). Synemin isoforms during mouse development: multiplicity of partners in vascular and neuronal systems. *Exp. Cell Res.* **315**, 769-783.
Jing, R., Wilhelmsson, U., Goodwill, W., Li, L., Pan, Y., Pekny, M. and Skalli, O. (2007). Synemin is expressed in reactive astrocytes in neurotrauma and interacts differentially with vimentin and GFAP intermediate filament networks. *J. Cell. Sci.* **120**, 1267-1277.
Kemp, M. W. and Davies, K. E. (2007). The role of intermediate filament proteins in the development of neurological disease. *Crit. Rev. Neurobiol.* **19**, 1-27.
Kemp, M. W., Edwards, B., Burgess, M., Clarke, W. T., Nicholson, G., Parry, D. A. and Davies, K. E. (2008). Syncoilin isoform organization and differential expression in murine striated muscle. *J. Struct. Biol.* **165**, 196-203.
Lariviere, R. C. and Julien, J. P. (2004). Functions of intermediate filaments in neuronal development and disease. *J. Neurobiol.* **58**, 131-148.
Lariviere, R. C., Nguyen, M. D., Ribeiro-da-Silva, A. and Julien, J. P. (2002). Reduced number of unmyelinated sensory axons in peripherin null mice. *J. Neurochem.* **81**, 525-532.
Le Marec, N., Caston, J. and Lalonde, R. (1997). Impaired motor skills on static and mobile beams in lurcher mutant mice. *Exp. Brain Res.* **116**, 131-138.
Lee, M. K., Xu, Z., Wong, P. C. and Cleveland, D. W. (1993). Neurofilaments are obligate heteropolymers in vivo. *J. Cell Biol.* **122**, 1337-1350.
Li, Z., Colucci-Guyon, E., Pincon-Raymond, M., Mericskay, M., Pournin, S., Paulin, D. and Babinet, C. (1996). Cardiovascular lesions and skeletal myopathy in mice lacking desmin. *Dev. Biol.* **175**, 362-366.
McCullagh, K. J., Edwards, B., Poon, E., Lovering, R. M., Paulin, D. and Davies, K. E. (2007). Intermediate filament-like protein syncoilin in normal and myopathic striated muscle. *Neuromuscul. Disord.* **17**, 970-979.
McCullagh, K. J., Edwards, B., Kemp, M. W., Giles, L. C., Burgess, M. and Davies, K. E. (2008). Analysis of skeletal muscle function in the C57BL6/SV129 syncoilin knockout mouse. *Mamm. Genome* **19**, 339-351.
McLean, J., Xiao, S., Miyazaki, K. and Robertson, J. (2008). A novel peripherin isoform generated by alternative translation is required for normal filament network formation. *J. Neurochem.* **104**, 1663-1673.
Mitchell, J. D. and Borasio, G. D. (2007). Amyotrophic lateral sclerosis. *Lancet* **369**, 2031-2041.
Nemeth, P. M. and Pette, D. (1980). The interrelationship of two systems of fiber classification in rat EDL muscle. *J. Histochem. Cytochem.* **28**, 193.
Newey, S. E., Howman, E. V., Ponting, C. P., Benson, M. A., Nawrotzki, R., Loh, N. Y., Davies, K. E. and Blake, D. J. (2001). Syncoilin, a novel member of the intermediate filament superfamily that interacts with alpha-dystrobrevin in skeletal muscle. *J. Biol. Chem.* **276**, 6645-6655.
Poon, E., Howman, E. V., Newey, S. E. and Davies, K. E. (2002). Association of syncoilin and desmin: Linking intermediate filament proteins to the dystrophin-associated protein complex. *J. Biol. Chem.* **277**, 3433-3439.
Rieger, F., Daniloff, J. K., Pincon-Raymond, M., Crossin, K. L., Grumet, M. and Edelman, G. M. (1986). Neuronal cell adhesion molecules and cytotactin are colocalized at the node of ranvier. *J. Cell Biol.* **103**, 379-391.
Robertson, J., Doroudchi, M. M., Nguyen, M. D., Durham, H. D., Strong, M. J., Shaw, G., Julien, J. P. and Mushynski, W. E. (2003). A neurotoxic peripherin splice variant in a mouse model of ALS. *J. Cell Biol.* **160**, 939-949.
Schefe, J. H., Lehmann, K. E., Buschmann, I. R., Unger, T. and Funke-Kaiser, H. (2006). Quantitative real-time RT-PCR data analysis: current concepts and the novel "gene expression's CT difference" formula. *J. Mol. Med.* **84**, 901-910.
Susuki, K. and Rasband, M. N. (2008). Molecular mechanisms of node of ranvier formation. *Curr. Opin. Cell Biol.* **20**, 616-623.
Tichopad, A., Pfaffl, M. W. and Didier, A. (2003). Tissue-specific expression pattern of bovine prion gene: quantification using real-time RT-PCR. *Mol. Cell. Probes* **17**, 5-10.
Tyc, F. and Vrbova, G. (2007). Modification of motoneuron size after partial denervation in neonatal rats. *Arch. Ital. Biol.* **145**, 337-344.
Xiao, S., McLean, J. and Robertson, J. (2006). Neuronal intermediate filaments and ALS: A new look at an old question. *Biochim. Biophys. Acta* **1762**, 1001-1012.
Xiao, S., Tjostheim, S., Sanelli, T., McLean, J. R., Horne, P., Fan, Y., Ravits, J., Strong, M. J. and Robertson, J. (2008). An aggregate-inducing peripherin isoform generated through intron retention is upregulated in amyotrophic lateral sclerosis and associated with disease pathology. *J. Neurosci.* **28**, 1833-1840.
Zhang, J., Bang, M. L., Gokhin, D. S., Lu, Y., Cui, L., Li, X., Gu, Y., Dalton, N. D., Scimia, M. C., Peterson, K. L. et al. (2008). Syncoilin is required for generating maximum isometric stress in skeletal muscle but dispensable for muscle cytoarchitecture. *Am. J. Physiol. Cell. Physiol.* **294**, C1175-C1182.
Zhu, Q., Couillard-Despres, S. and Julien, J. P. (1997). Delayed maturation of regenerating myelinated axons in mice lacking neurofilaments. *Exp. Neurol.* **148**, 299-316.